RESEARCH ARTICLE

An effective modification of $LiNi_{0.6}CO_{0.2}Mn_{0.2}O_2$ with $Li_{1.3}Al_{0.3}Ti_{1.7}(PO_4)_3$ as a high-performance cathode material for Li-ion batteries

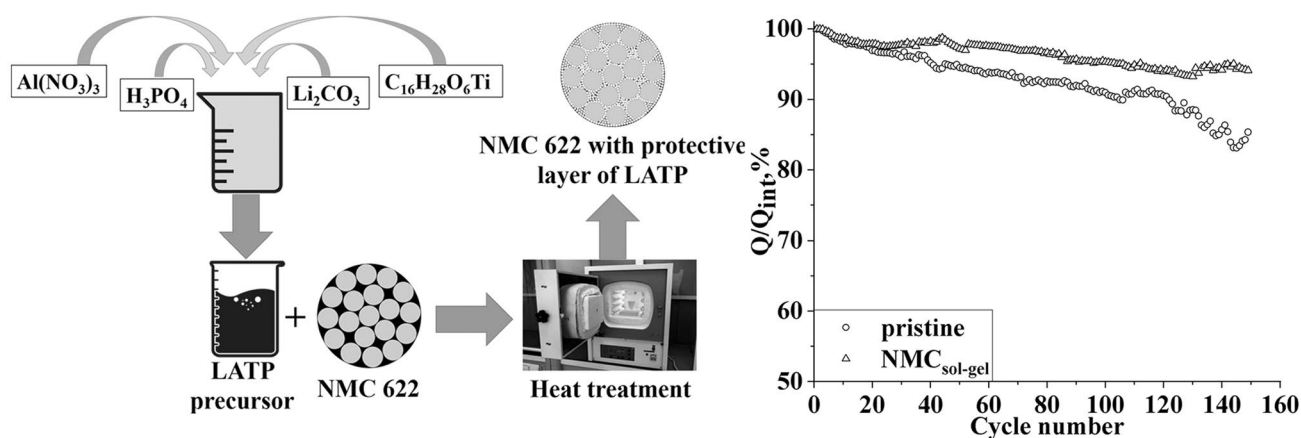I. V. Lisovskyi[1] · S. O. Solopan[1] · A. G. Belous[1] · V. G. Khomenko[2] · V. Z. Barsukov[2]

Abstract

$LiNi_{0.6}Co_{0.2}Mn_{0.2}O_2$ (NMC 622) cathode material is widely used for lithium-ion batteries. The effect of the method of creating a protective layer of $Li_{1.3}Al_{0.3}Ti_{1.7}(PO_4)_3$ (LATP) on the electrochemical characteristics of commercial cathode material NMC 622 was investigated. It was found that both methods of LATP coating did not affect the crystal structure and morphology of NMC 622. The prototypes of Li-ion batteries with a cathode based on modified NMC 622 are characterized by significantly higher stability of capacitive characteristics during long charge/discharge cycling, compared with prototypes of Li-ion batteries based on the pristine cathode material. In addition, the protective layer of LATP, applied by the sol–gel method, can significantly increase the capacity of the cathode material NMC 622 at the high current density and reduce the capacity drop during the continuous charge/discharge cycling. Creating a protective layer of LATP via sol–gel method is an effective way to improve the electrochemical characteristics of cathode materials such as NMC 622.

Graphical abstract

✉ I. V. Lisovskyi
i-lisovskii@i.ua

1   V. I. Vernadsky Institute of General and Inorganic Chemistry of the NAS of Ukraine, 32/34 Academic Palladin Avenue, Kiev 03142, Ukraine

2   Kyiv National University of Technologies and Design, 2 Nemyrovycha-Danchenka Street, Kiev 01011, Ukraine

1 Introduction

Lithium-ion batteries (LIBs) are widely used in consumer electronics, mobile phones, personal computers, as well as in hybrid and electric vehicles [1]. Various Li-containing materials are used as cathode materials for LIB, such as $LiCoO_2$, $LiNiO_2$, $LiMnO_2$, and so on. The most common cathode material in the commercial LIBs is lithium cobaltite

($LiCoO_2$). The main disadvantages of $LiCoO_2$ are high cost and low specific capacity (130–140 mAh/g) [2]. NMC solid solutions that chemical formula is $LiNi_xCo_yMn_zO_2$ ($0 < x$, y, $z < 1$, $x + y + z = 1$) are promising candidates for replacing lithium cobaltite. They are characterized by the higher capacity compared to $LiCoO_2$, better thermal stability during the interaction with the electrolyte than $LiNiO_2$, and better stability in cycling than $LiMnO_2$ [3, 4]. However, according to the literature data, both the charge–discharge capacity and thermal stability for NMC-type layered cathode materials strongly depend on the ratio of nickel, cobalt, and manganese in their structure. For example, it is well known that high nickel content promotes the increase in capacity but reduces the level of safety, while high content of cobalt and manganese improves the cyclicity and safety level by the reducing power [5, 6]. Therefore, the optimization of the chemical composition of NMC is a very important task for the enhancement of the electrochemical characteristics and safety level of LIBs using NMC-type cathode materials.

NMC-type materials, as well as other cathode materials, suffer from an interphase reaction between the cathode material and the liquid electrolyte, which results in the transition of Co^{3+} to Co^{4+} and destruction of the NMC structure due to the disordering Li^+ and Ni^{2+} ions in the crystalline lattice [7]. This interaction reduces the specific power and impairs the cyclicity of the cathode material. In addition, the literature data also notes that overcharging an NMC-based battery leads to the reducing Ni^{4+} to Ni^{2+}, which is accompanied by the oxygen release and, due to the device overheating and interaction with flammable electrolyte, can lead to the explosion or ignition of the battery [8, 9]. The safety issue connected with the oxygen evolution is considered as the main disadvantage of using cathode materials with a high nickel content, despite of the obvious advantage of high capacity. One of the most promising NMC-type layered cathode materials with a high nickel content is the material, which has the chemical composition of $LiNi_{0.6}Co_{0.2}Mn_{0.2}O_2$ (NMC 622) [10, 11]. This material is characterized by the stable characteristics, high discharge–charging capacity, and a high level of safety, even at elevated temperatures [12, 13].

To prevent the interfacial side reactions, composite systems, in which a shell of chemically stable (in contact with the electrolyte) and electrochemically inert materials (such as $FePO_4$, Al_2O_3, $AlPO_4$, and so on) is applied to the particles of the NMC cathode material, were proposed [14–21]. Such a protective layer must be dense enough to prevent the contact of the cathode material with the liquid electrolyte and, at the same time, its thickness should not exceed a few nanometers, so as not to interfere the migration of lithium-ions through it. In [22], the authors showed that solid electrolytes, in particular lithium-aluminum-titanium phosphate $Li_{1.3}Al_{0.3}Ti_{1.7}(PO_4)_3$ (LATP) with NASICON structure, can be used to create a protective shell on the particles of

cathode materials. The protective layer was applied by the mechanical mixing NMC 532 particles and pre-synthesized LATP nanoparticles for 24 h in cyclohexane. This allowed achieving a significant improvement in the stability of the capacitive characteristics of the cathode material during a continuous discharge/charge cycle.

The deposition method [23, 24] and the sol–gel method [25] are often used to apply a protective shell of simple oxides to the cathode material. These methods are traditionally used in the coating oxide materials such as TiO_2, ZrO_2, or SiO_2, but they are quite difficult to implement for more complex systems such as $AlPO_4$ or $FePO_4$ [26, 27]. At the same time, it is difficult to achieve a uniform deposition of an all-over protective layer on the particles of the cathode material when creating a protective layer by the mechanical stirring, since the particles of the protective layer in the most cases are unevenly distributed. However, there are no data in the literature on the relationship between the method of creating a protective layer on the surface of the particles of cathode materials and its electrochemical characteristics.

The aim of this work was to create a protective layer of LATP nanoparticles on the surface of particles of commercial cathode material NMC 622 using two methods (mechanical mixing and sol–gel method) and to study the effect of the method of creating a protective layer on the electrochemical characteristics of the cathode material.

2 Experimental

Obtaining $Li_{1.3}Al_{0.3}Ti_{1.7}(PO_4)_3$ via *sol–gel method*. LATP nanoparticles, which were used for the creation of a protective layer on the surface of the cathode material, were synthesized by the sol–gel method. Lithium carbonate Li_2CO_3 (99.99% Merck), aqueous solution of aluminum nitrate $Al(NO_3)_3$ (99.99% Merck), diacetylacetonate diisopropylate (IV) titanium $C_{16}H_{28}O_6Ti$ (~75% in isopropanol) (purum, Sigma-Aldrich), 85% orthophosphoric acid H_3PO_4 (in water, FCC, FG Sigma-Aldrich), 65% nitric acid HNO_3 (Sigma-Aldrich), 25% aqueous solution of ammonia NH_4OH (99% Sigma-Aldrich), citric acid (CA) (anhydrous, 99%, Merck), and ethylene glycol (EG) (99% Sigma-Aldrich) were used as the starting reagents for the synthesis. A stoichiometric amount of Li_2CO_3 was dissolved in 5 ml of nitric acid and added to the stoichiometric volume of aluminum nitrate solution. Appropriate amounts of citric acid and ethylene glycol were added to the aluminum and lithium solution and the mixture was heated at 120 °C with constant stirring. Titanium diacetylacetonate diisopropylate (IV) was added after the evaporation of the solution for 8 h., Orthophosphoric acid and aqueous ammonia solution were added one hour after the addition of the titanium solution to achieve pH = 10. The synthesis was continued for 10 h at a temperature of

135 °C up to the gel formation. LATP precursor powder was obtained after pyrolysis of the gel at a temperature of 350–450 °C. To form the crystalline structure of the particles, the pyrolysis product (LATP precursor) was treated at 750° C for 2 h.

Application of a protective layer of $Li_{1.3}Al_{0.3}Ti_{1.7}(PO_4)_3$ *on particles of the cathode material.* A commercial sample of $LiNiCoMnO_2$ (Ni:Co:Mn = 6:2:2, hereinafter NMC 622) manufactured by MTI Co was used as the cathode material. The LATP protective layer on the surface of the NMC 622 cathode material particles was formed using two methods—mechanical mixing and sol–gel technology. In [22], the authors demonstrated the effect of applying different amounts of LATP protective coating on the properties of the cathode material NCM 532 and showed that the optimal ratio of cathode material to the amount of LATP nanoparticles applied to the surface of the cathode material is 99: 1 wt. %. Therefore, similar ratios of LATP nanoparticles and cathode material were used in this work.

To apply a protective LATP layer by the mechanical stirring (Fig. 1), the pristine particles of the commercial cathode material NMC 622 and the pre-synthesized LATP nanoparticles in a ratio of 99:1 wt. % were homogenized in isopropanol for 24 h by an alternating stirring on a magnetic stirrer and ultrasonic homogenization at the room temperature. The obtained suspension was dried up to the complete removal of the solvent and heat-treated at 750 °C for 2 h with the heating rate of 5 °C/min.

To apply a protective layer of LATP on the particles of the cathode material by the sol–gel method, NMC 622 particles were injected into the jar, in which the LATP synthesis was carried out, according to the scheme shown in Fig. 2.

To establish the effect of the method of creating a protective layer of the cathode material on its electrochemical characteristics, the following samples were studied:
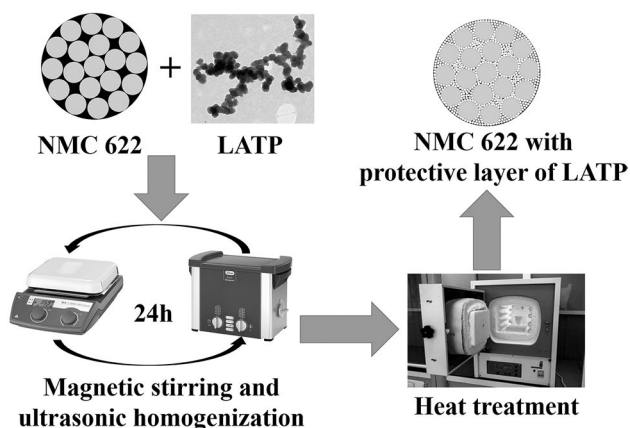

Fig. 1 Scheme for applying a protective layer of LATP on particles of commercial cathode material NMC 622 by the mechanical mixing
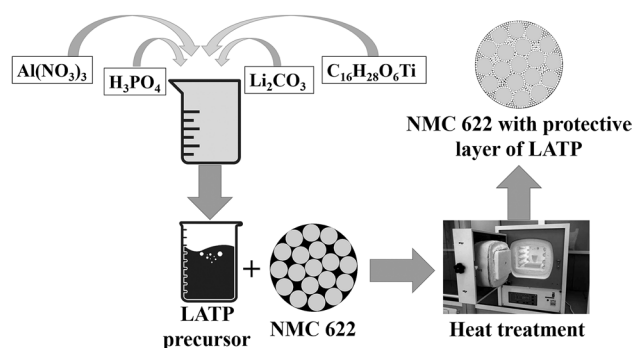

Fig. 2 Scheme for applying a protective layer of LATP on particles of the commercial cathode material NMC 622 via sol–gel method

- NMC 622 without LATP protective layer (pristine);
- NMC 622 with LATP protective layer applied by the homogenizing pre-synthesized LATP nanoparticles with the particles of cathode material in isopropanol for 24 h (NMC_m);
- NMC 622 with LATP protective layer applied by the homogenization of pre-synthesized LATP nanoparticles with particles of cathode material in isopropanol for 24 h, followed by the heat treatment of the composite for 2 h at a temperature of 750 °C (NMC_m (T));
- NMC 622 with a protective layer of LATP, applied by the injection of cathode material particles into the reaction jar during the synthesis of LATP sol–gel method, followed by the heat treatment of the composite for 2 h at a temperature of 750 °C ($NMC_{sol-gel}$).

Production of LIBs models. The cathode mass was prepared by stirring the cathode material (pristine NMC or NMC/LATP composite) with PVDF (polyvinylfluoride) solution in N-methyl pyrrolidone, carbon black, and graphite at a ratio of 85:7:4:4 wt%.. Graphite SFG-6L and carbon black C65 were obtained from Timcal, Switzerland. The suspension was applied to the 20 μm thick aluminum current collector using a Doctor Blade applicator. To remove the organic solvent, the collector with the applied cathode mass was dried for 30 min at a temperature of 100 °C. The electrode was rolled through rollers to seal the cathode material. The electrodes were cut in the form of disks with the diameter of 16 mm and additionally dried at a temperature of 120 °C for 12 h. The lithium electrode was made in a glove box from MBraun (USA) filled with argon. The content of water vapor and molecular oxygen in the box did not exceed 5 ppm. The anodes were cut from 0.4 mm thick lithium tape in the form of disks with a diameter of 16 mm. Experimental LIBs were built using casing parts CR2016 coin-type cells. Separator Celgard 2400 with a thickness of 25 μm saturated with the electrolyte (1 M solution of $LiPF_6$ in a mixture of solvents—ethylene carbonate/dimethyl carbonate/diethylene

carbonate in a ratio of 1:1:1) was placed in the case of the element.

Design of LIBs prototypes. It is well known that the cycling of half-cells with a lithium electrode is limited by the behavior of the lithium electrode due to the formation of dendrites and the resulting increase in resistance. Therefore, the issues related to the design of prototypes of lithium-ion batteries and their suitability for the study of LIBs' materials in various types of tests, including long-term cycling, were investigated in this work. Casing parts of CR2016 coin-type cells using tape electrodes were used to implement LIBs' prototypes. The following parameters were taken into account during the research and development work on the design of the lithium-ion batteries: a) the need to properly balance the capacity of the positive and negative electrodes; b) it is necessary to achieve the highest values of specific energy and specific power. The test and layout focused on the electrochemical system with graphite anode based on TIMCAL TIMREX® SLP30 and cathodes based on pristine NMC and NMC$_{sol-gel}$.

Equipment. The phase composition of the samples was determined by X-ray diffraction method (XRD) using DRON-4-07 diffractometer (CuKα-radiation, Ni-filter). Certified SiO$_2$ (2θ standard) and Al$_2$O$_3$ (intensity standard) were used as the external standards [21]. Crystallographic lattice parameters of the samples were calculated by Rietveld method using FULL-PROF software package. The degree of crystallinity of the particles was calculated by the XRD integration method.

The morphology of the powders was observed using a JEM 1400 transmission electron microscope (Jeol, Japan) and a SEC miniSEM SNE 4500 MB scanning electron microscope. EDS spectra and element distribution maps were recorded using the EDAX Element PV6500/00 F.

The charge/discharge characteristics of LIBs models were obtained using multi-potentiostate ARBIN (MITS Pro Software of MSTAT 32, Arbin Corporation, USA) and VMP3 (Bio-Logic-Science Instruments, France). To establish the repeatability of the results, a set of three cells with the same composition of the cathode material was investigated.

3 Results and discussion

XRD results for materials obtained during the synthesis of LATP by the sol–gel method (Fig. 3a) show that LATP precursor is amorphous during the synthesis, and the formation of a crystalline NASICON-type structure occurs in one stage at the temperatures above 750 °C. Crystallographic parameters calculated via XRD show that the synthesized samples have a rhombohedral structure and belong to the space group of $R\bar{3}c$ with the next cell parameters: a = 8.503 Å; c = 20.787 Å; V = 1301.46 Å^3. Figure 3b represents TEM
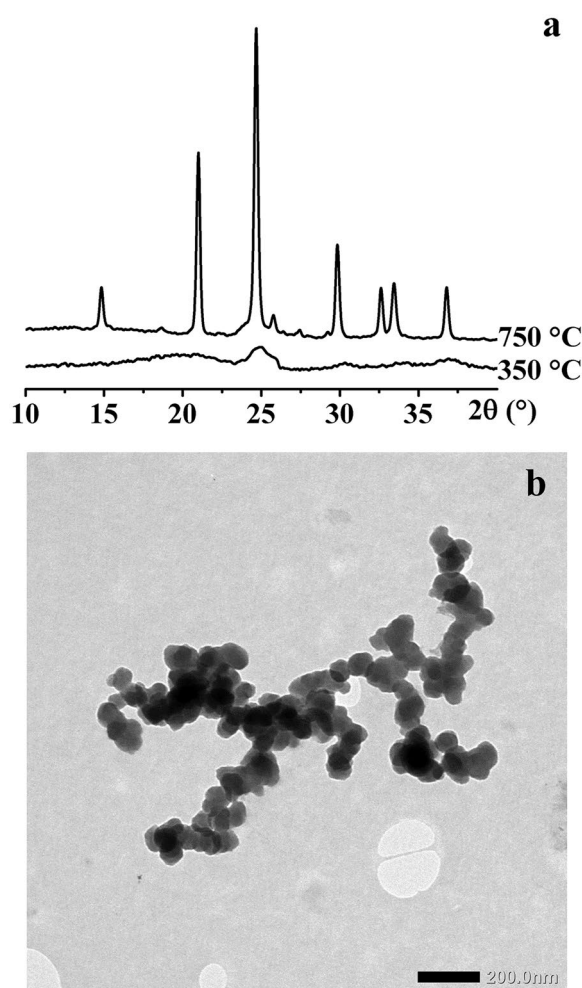
Fig. 3 XRD patterns (**a**) and TEM image (**b**) of LATP nanoparticles obtained by the sol–gel method

image, which shows that nanoparticles are weakly agglomerated and their size varies in the range from 50 to 80 nm.

Figure 4 demonstrates the results of X-ray phase analysis of both the pristine cathode material NMC and LATP nanoparticles synthesized by the sol–gel method (Fig. 4a), and cathode materials with a protective layer of LATP (1 wt.%), applied by two methods (Fig. 4b). All NMC diffraction peaks can be indexed in a hexagonal-layered structure of the α-NaFeO$_2$ type with a space group of $R\bar{3}m$ that is evidenced by the clear splitting of the (006)/(012) peaks, and LAT—in a rhombohedral structure with a space group of $R\bar{3}c$. Peaks of the NASICON rhombohedral structure are not observed in the XRD patterns of the cathode materials with a protective LATP layer due to the low LATP content in the investigated systems.

Crystal lattice parameters for NMC, NMC$_m$, NMC$_m$ (T), and NMC$_{sol-gel}$ samples calculated by the Rietveld method are shown in Table 1. Here, R$_b$ is Bragg factor and R$_f$ is compliance form factor [29]. As can be seen from the table, the
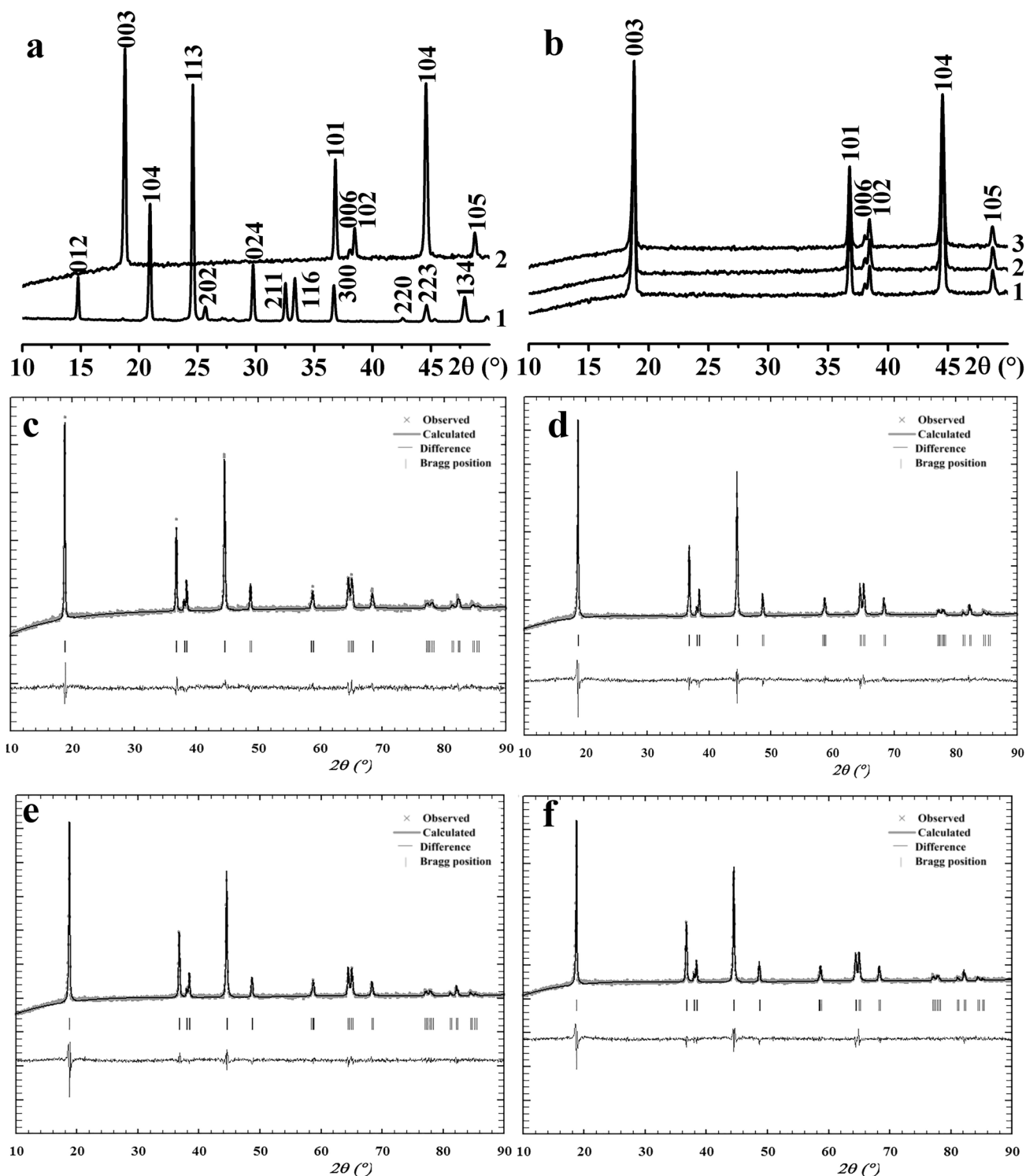
Fig. 4 XRD patterns for (**a**) LATP (1) and pristine NMC (2) materials; **b** cathode materials coated with a LATP protective layer by various methods: 1—NMC$_m$; 2—NMC$_m$ (T); 3—NMC$_{sol-gel}$. Observed and calculated XRD patterns of samples: **c**—pristine NMC; **d**—NMC$_m$; **e**—NMC$_m$ (T); **f**—NMC$_{sol-gel}$

unit cell size for all samples is slightly different. This may indicate that Ti^{4+} ions present in the structure of the LATP protective layer diffuse into the structure of the cathode material during the coating process, which is also indicated by the authors of a number of works [29–31]. Increasing the parameters of the crystal lattice leads to an increase in

Table 1 Structural parameters obtained from Rietveld Refinement of pristine and LATP-coated samples

Sample	a (Å)	c (Å)	V (Å^3)	c/a	R_b	R_f	Crystallinity, (%)
Pristine	2.8634	14.1921	100.812	4.955	2.20	2.17	88.96
NMC$_m$	2.8656	14.2050	101.017	4.957	2.78	2.14	85.72
NMC$_m$ (T)	2.8667	14.2102	101.127	4.957	2.55	2.15	89.81
NMC$_{sol\text{-}gel}$	2.8687	14.2197	101.343	4.957	2.66	2.18	91.82

the size of the diffusion channels of lithium-ion that simplifies the intercalation and deintercalation of lithium and reduces the destruction of the material during cycling [32]. At the same time, the table shows the ratio of the parameters c/a. According to the authors [28, 31], the value of c/a is an important factor that indicates the layered nature of the material structure. When the value of c/a is greater than 4.9, there will be a layered structure in the material. The greater this value, the greater the proportion of layered structure. As can be seen from the table, the value of c/a for all cathode materials is ~ 4.95 and practically does not change with the application of a protective layer. This indicates that the samples with a protective layer of LATP retain their original crystalline structure.

Also, in the table, the values of crystallinity of the investigated samples are given. As can be seen from Fig. 5, the particles of the cathode material have a spherical shape and are porous, and the degree of their crystallinity is not equal to 100%. At the same time, when applying the LATP protective layer in the case of mechanical application, there is a decrease in the degree of crystallinity of the particles, which may indicate a statistical distribution of LATP particles on the surface of the cathode material. Since LATP particles are nanosized, this will reduce the degree of crystallinity of such composite structures. During heat treatment of such composite structures, LATP nanoparticles close the pores of the cathode material, which leads to an increase in the degree of crystallinity. In the case of the NMC sample, the gel penetrated into the surface layers of the porous structure of the cathode material, thereby reducing the number of pores and defects in such structures, which led to an increase in the degree of crystallinity of the composite structures.

The morphology of the pristine cathode material NMC 622 and the cathode material with a protective LATP layer was examined using scanning electron microscopy, and obtained results are shown in Fig. 5. As it can be seen in this figure (Fig. 5a), the particles of the pristine cathode material have a spherical shape and a size near 7 μm. The surface of the particles is porous. It is not homogeneous and consists of a large number of particles with a size near 500 nm. In contrast to the pristine cathode material, a large number of smaller particles are observed on the surface of NMC particles with a protective layer (Fig. 5b, c), and their surface is more homogeneous. According to the results of energy dispersion spectroscopy (EDS), there are no peaks

of aluminum, titanium, and phosphorus on the surface of the particles of the pristine cathode material. At the same time, there are distinct signals of these elements in the EDS spectra of the particles with a protective layer of LATP. Thus, the performed studies demonstrate that using both methods (mechanical application method and sol–gel method) allows obtaining a continuous protective layer of LATP on the surface of the particles of the cathode material.

Electrochemical investigation of LIBs models. To study the electrochemical properties of modified cathode materials, LIB models testing was performed, and its schematic representation is shown in Fig. 6.

The results of the study of cyclic voltammetry (CVA) of the first 3 cycles of laboratory models of electrochemical cells with different samples of cathode materials in the voltage range 2.7–4.5 V are shown in Fig. 7. The curves were obtained at the room temperature and the potential sweep rate of 0.01 mV/s. The CVA method is used to assess the reversibility of intercalation–deintercalation of the process of electrochemical incorporation of lithium into the cathode material. For the first cycle, one pair of cathode/anode peaks is observed, which indicates on the one-stage Red-Ox processes for these materials. Upon subsequent cycling, there is an expansion of the peak in the cathode region. The reason for this may be due to the decrease in the crystallinity of the cathode material with the incorporation of lithium-ions. The results of the study point on the effect of heat treatment on the process of amorphization of the material during the cycling.

It should be noted that in the first cycle, the specific charge of the anode half-cycle of the CVA exceeds the corresponding value of the cathode half-cycle. This is due to the formation of a passivating film on the surface of the cathode material, which is formed in the first and partially in the second cycle. During subsequent cycling, the specific charge of the anode and cathode half-wave of CVA is the same, and the Coulomb efficiency is almost 100%, which indicates the absence of adverse reactions. However, the current response (Fig. 7b–d) is associated with a pronounced peak shift in the direction of the scan. On the other hand, all electrodes with LATP show good reversibility of the charge transfer. Therefore, the slight separation of peaks in CV cannot be interpreted by the redox processes in LATP. A pronounced peak shift indicates that Li + intercalation in composite NMC-LATP happens under charge transfer and

Fig. 5 SEM images and EDS results for the pristine cathode material NMC and LATP-coated cathode material using different methods: **a**—pristine NMC 622; 6—NMC_m (T); **b**—$NMC_{sol–gel}$
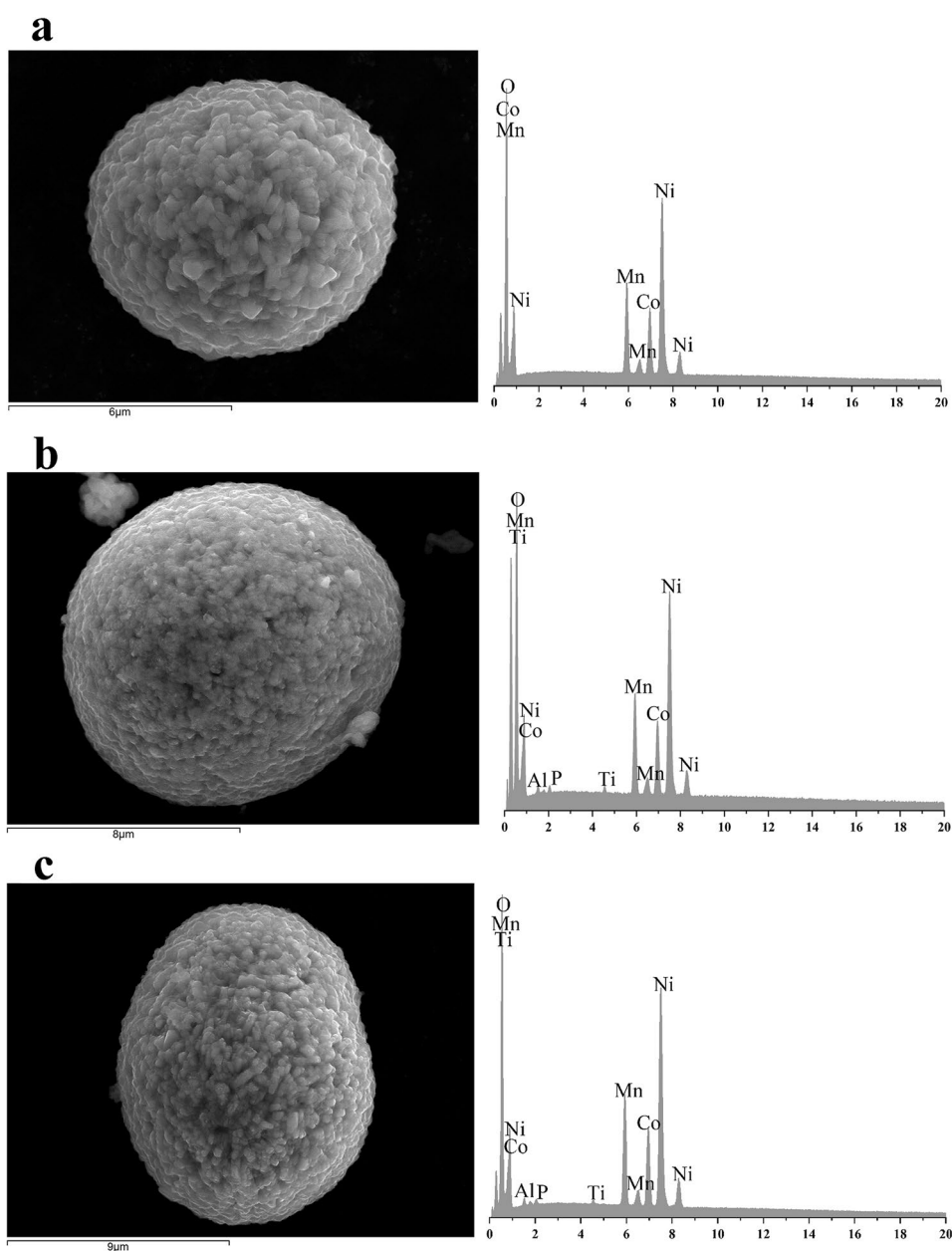
diffusion contributes to the electrochemical response. The solid-state diffusion was modified by LATP. The relative contributions of charge transfer and solid-state diffusion in composite NMC-LATP are not constant in the voltage. This aspect is better inferred from EIS data.

Nyquist diagrams of LIBs models with cathodes based on the pristine NMC, NMC_m, NMC_m (T), and $NMC_{sol-gel}$, which correspond to the state of charge of the cathode material, are shown in Fig. 8. The Nyquist curves are well described by the scheme in Fig. 9 and the simulation results are shown in Table 2. Impedance spectroscopy data are obtained in charged and discharged states of the cathode material. Elements describing the behavior of the cathode material (W,

CPE_1, R_c) are included in the equivalent circuit in order to better describe the processes occurring at the electrode/electrolyte interface. The influence of the electrode/separator interface (R, C) and the influence of the lithium counter electrode (CPE_2, R_{Li}) are also taken into account. Sometimes, in a half-cell system, the impedance value is coming from the lithium counter electrode. In order to minimize this effect on impedance spectrum, SEI was obtained after initial cycling of cells. In this case, the lithium counter electrode causes a relatively lower impedance (CPE_2, R_{Li}). Thus, R_e and R_c represent the bulk resistance of electrolyte and the charge transfer resistance, respectively. The inclined line at low frequency is derived from Warburg impedance (W), which is
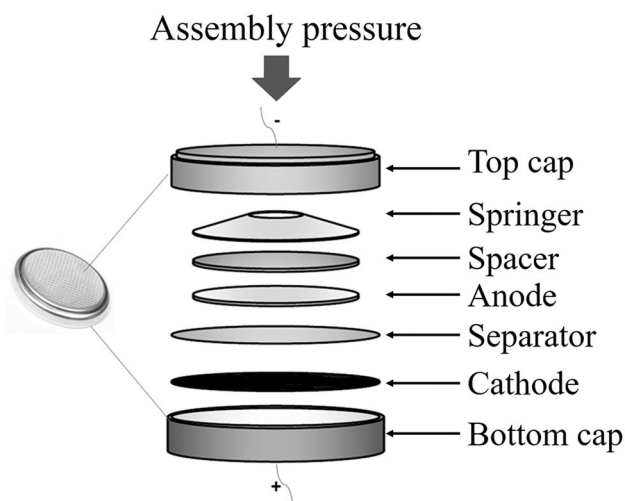
Fig. 6 Schematic representation of laboratory models of LIB for the investigation of cathode materials

related to lithium-ion diffusion within cathode. According to table, the lower value of the charge transfer resistance (R_c) is acquired in a discharged state of cathode which corresponds to the higher concentration of Li^+ ions in cathode. After charging of cathode up to 4.5 V, Li^+ ions are extracted from the cathode that is accompanied with an increase of R_c.

It was found that the R_c value is higher for the elements based on of the pristine cathode material and NMC_m after analyzing the simulation results. Consequently, the elements based on NMC_m (T) and $NMC_{sol-gel}$ exhibit a much lower R_c value than pristine NMC, indicating the deposited LATP enhanced Li^+ transport across cathode/electrolyte interface. Due to the fact that the semicircle (Fig. 8) is compressed, and a constant phase element CPE_1 is represented inhomogeneity on electrode/electrolyte interface, surface roughness, and electrode porosity as well. According to our data, LATP does not lead to degradation of the cathode surface due to the formation of a thicker SEI and, therefore, cannot affect the charge/discharge process. Totally, the CPE of samples
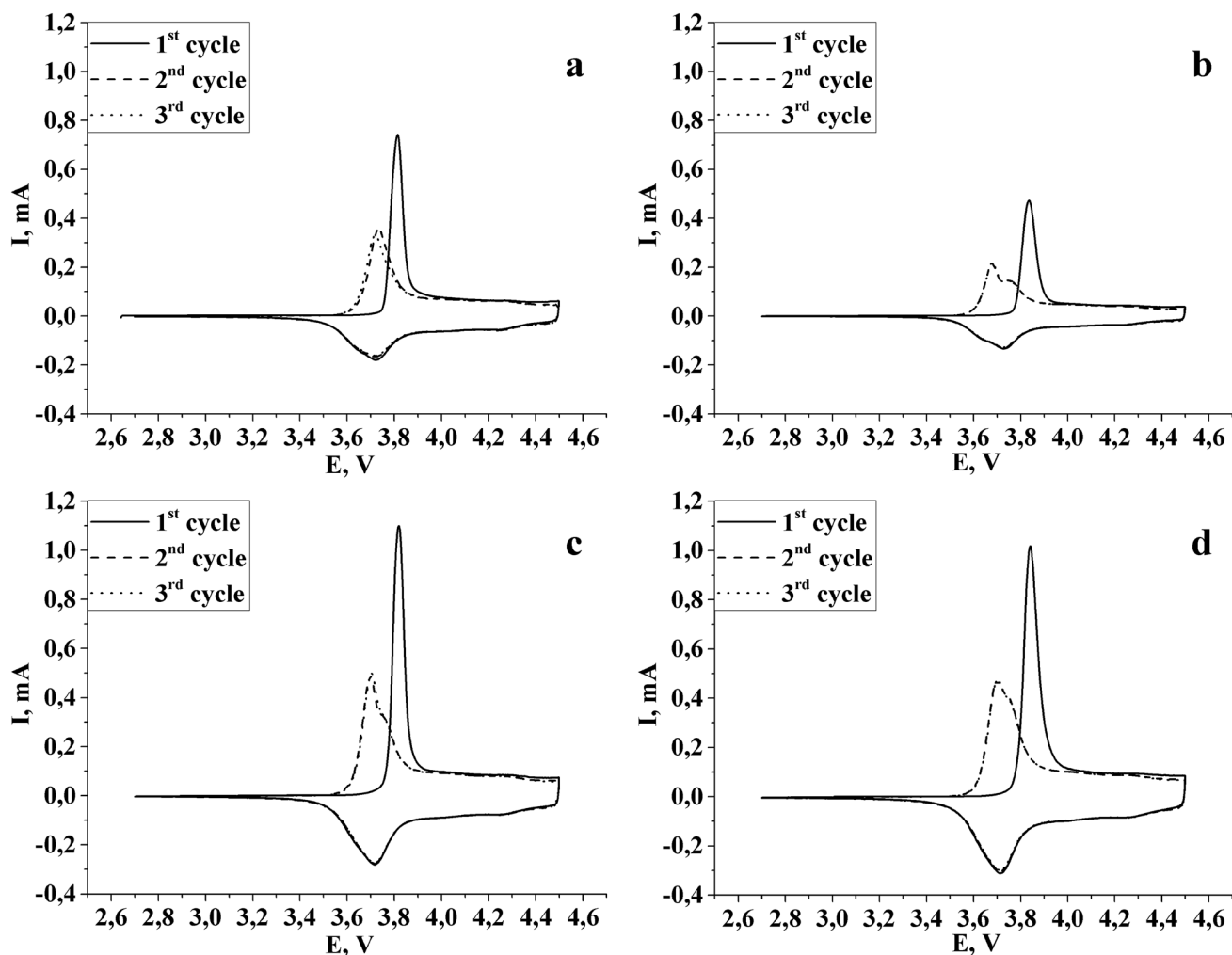

Fig. 7 CVA of pristine and composite cathode materials: **a**—pristine NMC; **b**—NMC_m; **c**—NMC_m (T); **d**—$NMC_{sol-gel}$
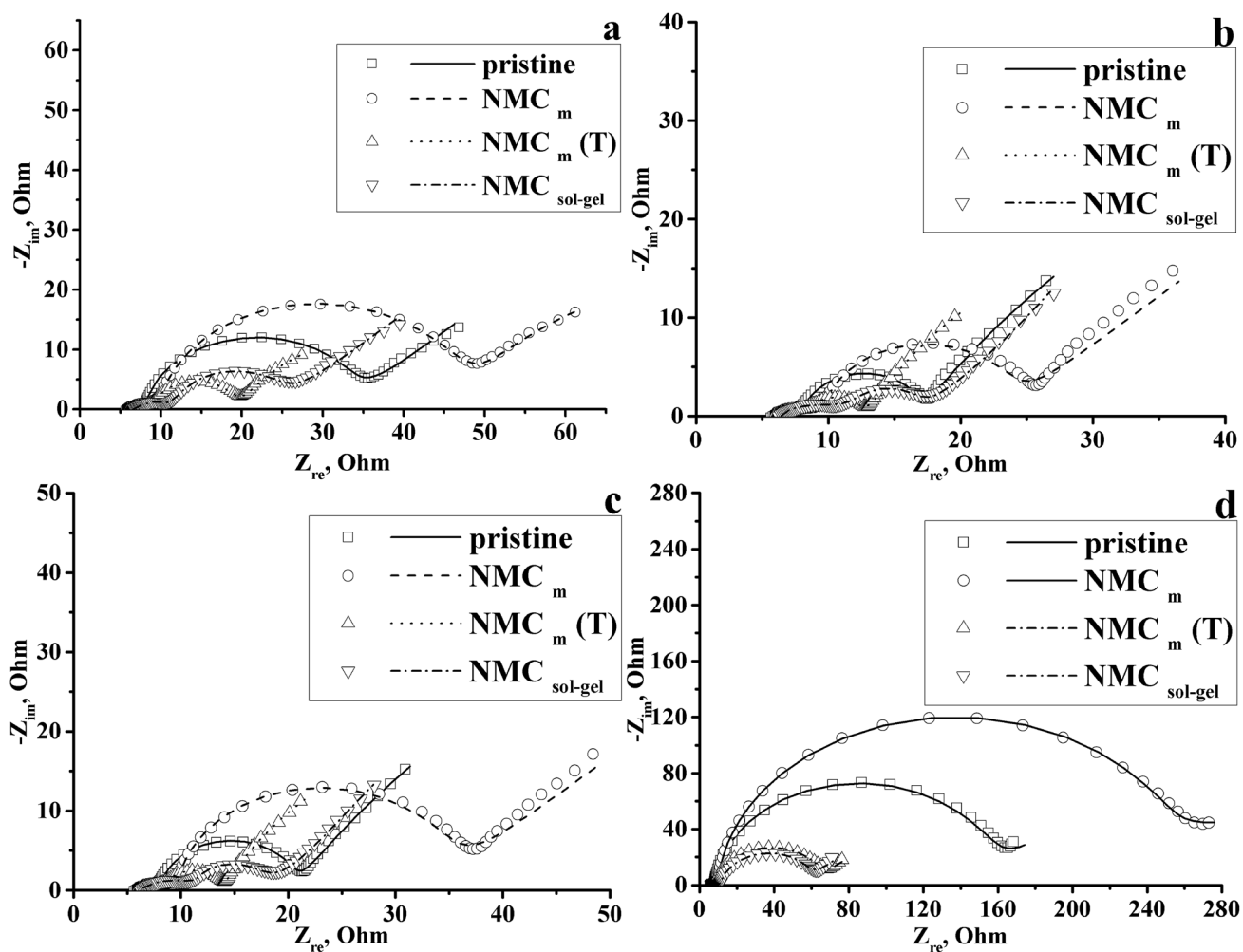
Fig. 8 Nyquist diagrams of the pristine and composite cathode materials at different potentials vs Li: **a**—3.7 V; **b**—4.0 V; **c**—4.2 V; **d**—4.5 V
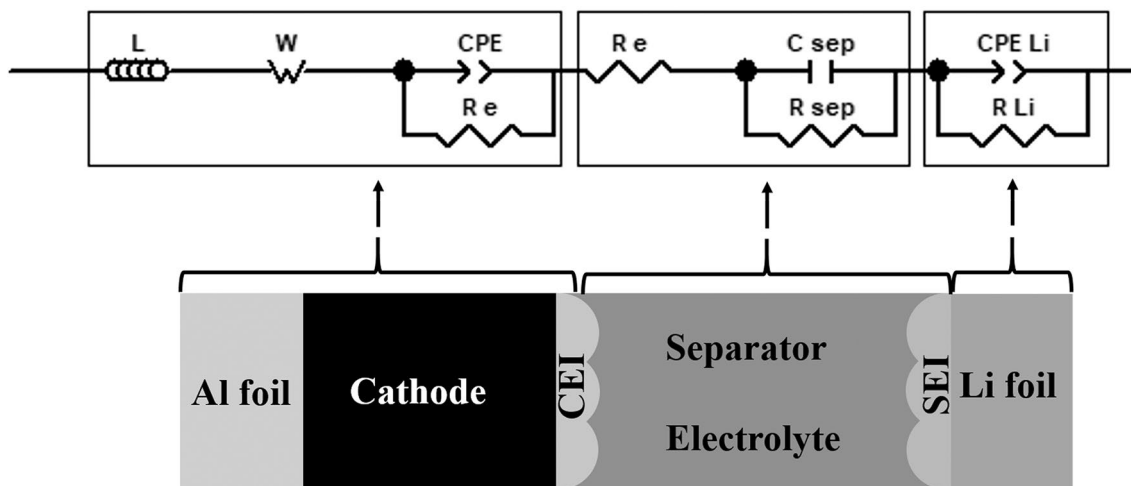

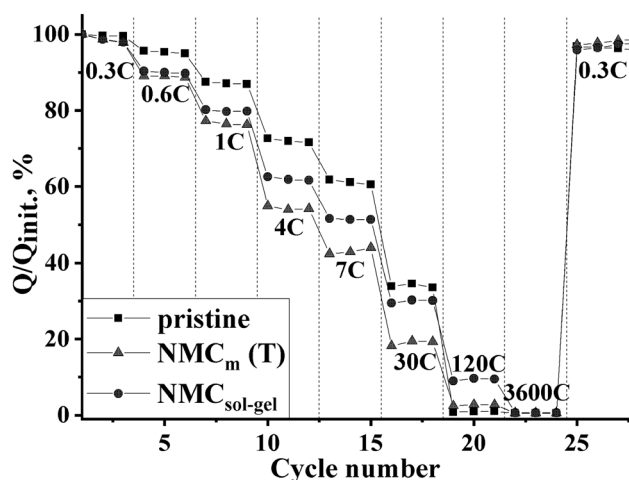**Fig. 9** Equivalent circuit used for simulating the experimental impedance data

Table 2 Results of EIS-fitting of the equivalent circuit of an electrochemical cell with a lithium anode and NMC-based cathode from pristine and composite cathode materials

	4.5 V				3.7 V			
	NMC	NMC_m	NMC_m (T)	$NMC_{sol-gel}$	NMC	NMC_m	NMC_m (T)	$NMC_{sol-gel}$
L, Hcm^2	3.41E-07	2.64E-07	3.53E-07	2.67E-07	2.77E-07	2.83E-07	3.14E-07	2.65E-07
R_e, $\Omega\,cm^2$	5.24	6.63	5.18	5.86	5.67	6.73	6.32	6.83
W, $\Omega^{-1}\,s^{-0.5}\,cm^{-2}$	0.116	0.258	0.170	0.176	0.201	0.170	0.318	0.189
CPE_1, $\Omega^{-1}s^n cm^{-2}$	0.0034	0.0037	0.0051	0.0066	0.0033	0.0036	0.0051	0.0064
n	0.97	0.95	0.94	0.86	0.95	0.95	0.89	0.87
R_c, $\Omega\,cm^2$	142.8	254.7	53.42	48.28	24.07	34.52	9.614	12.98
CPE_2, $\Omega^{-1}s^n cm^{-2}$	0.0004	0.0006	0.0005	0.0006	0.0006	0.0010	0.0005	0.0003
n	0.70	0.73	0.74	0.74	0.74	0.67	0.73	0.71
R_{Li}, $\Omega\,cm^2$	1.80	1.20	1.42	1.71	1.84	2.44	1.96	3.94
C, Fcm^{-2}	0.0069	0.0069	0.0069	0.0069	0.0069	0.0069	0.0069	0.0069
R, $\Omega\,cm^2$	0.38	0.38	0.38	0.38	0.38	0.38	0.38	0.38
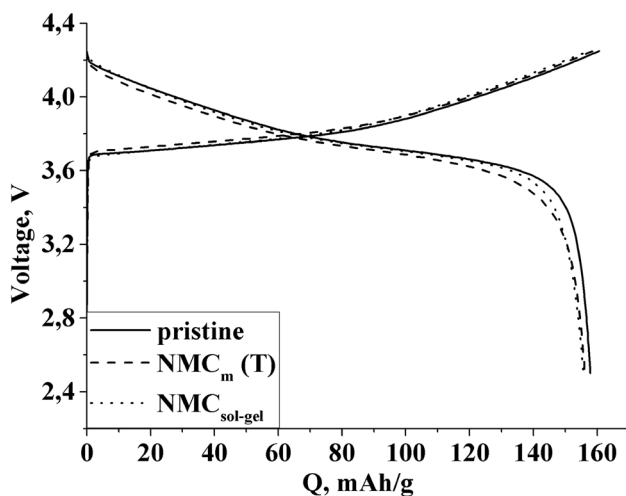
Fig. 10 Charge/discharge curves of pristine and composite cathode materials

Fig. 11 The specific capacity of the pristine cathode material and cathode materials with a protective layer of LATP at the different current densities

NMC_m (T) and $NMC_{sol-gel}$ did not increase sufficiency that confirms out conclusions from the rate capability test.

The results of studies of galvanostatic charge–discharge cycling of electrochemical cells with cathodes made of the pristine NMC 622, NMC_m (T) and $NMC_{sol-gel}$ in the voltage range of 2.4–4.2 V and at a current density of C/5 are shown in Fig. 10. Galvanostatic curves correlate well with the results of the CVA study. The calculated specific values of the accumulated charge are as follows: for the pristine material—158 mAh/g; for NMC_m (T) and $NMC_{sol-gel}$, this parameter is 157 and 156 mAh/g, respectively. According to the results of the study (Fig. 10) of the NMC and LATP composites, it was found that the modification of the cathode

material with LATP nanoparticles does not cause the large losses in the specific capacity of the cathode material. A slight reduction in the specific capacity relative to the pristine cathode material is due to the replacement of part of the NMC in the cathode by inactive LATP.

Figure 11 shows the dependence of the specific capacity on the charge/discharge current density of the pristine cathode material NMC 622 and cathode materials with a protective layer of LATP in the voltage range from 2.5 to 4.2 V. It is obvious that the specific capacity of all samples decreases with the increasing current density. It should be noted that the specific capacity of cathode materials with

a protective layer is lower than the specific capacity of the pristine cathode material at low current densities. This may be due to the replacement of the part of the NMC in the cathode with inactive LATP. However, the specific capacity of the NMC$_{sol-gel}$ is significantly higher than that of other materials (pristine NMC 622 and NMC$_m$ (T)) at current densities more than 30C. There are technical limitations to testing at a higher current rate. The effects of the counter electrode and the low electrical conductivity of the electrolyte are decisive. The above effect limits the performance of cells. Comparable test at over 1C shows that the application of a protective layer of LATP via sol–gel method can significantly increase
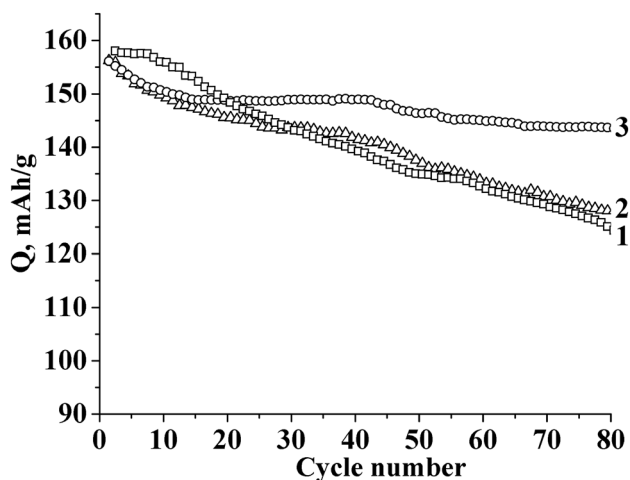
the specific capacity of the cathode material NMC 622 at the high current densities.

Figure 12 shows the results of galvanostatic cycling of LIBs models with cathodes based on the pristine NMC, NMC$_m$ (T), and NMC$_{sol-gel}$ at a temperature of 12 °C in the voltage range of 2.7—4.3 V instead of 4.2 V which is commonly used. Reducing the temperature and increasing the cycling voltage allows better determination of the action of the protective layer, since these changes lead to an increase in the rate of degradation of the characteristics of the cathode material [33, 34]. Figure 12 shows that at the beginning of the cycling the capacity of both composite cathode materials is inferior to the cathode material without a protective layer, but the capacity drop during the cycling process for the capacity cathode material is much lower. The capacity drop of the cells during long cycling is primarily due to the poor cycling stability of the lithium electrode [35] and the formation of dendrites on its surface. The decision to limit the study to 80 cycles was made for the same reason.

LIBs prototypes with a capacity of 3–5 mAh with a maximum voltage of 4.3 V at a current density of C/5 were constructed and investigated. Cycle curves for LIBs prototypes are shown in Fig. 13. The charge/discharge curves for LIBs prototypes with pristine and modified NMC are similar. It should be noted that significantly higher values of residual capacity were observed after long cycling for the LIBs prototype with cathode material, NMC$_{sol-gel}$ material. For example, during 150 cycles, the LIBs prototypes made using NMC$_{sol-gel}$ as a cathode material lost 7.14% of the initial capacity, while, for the LIBs prototypes with the pristine cathode material, this value was 16.74%. Changing the capacity during cycling is shown in Fig. 14. The figure shows that LIBs prototypes with a cathode based on NMC$_{sol-gel}$ were characterized by significantly higher

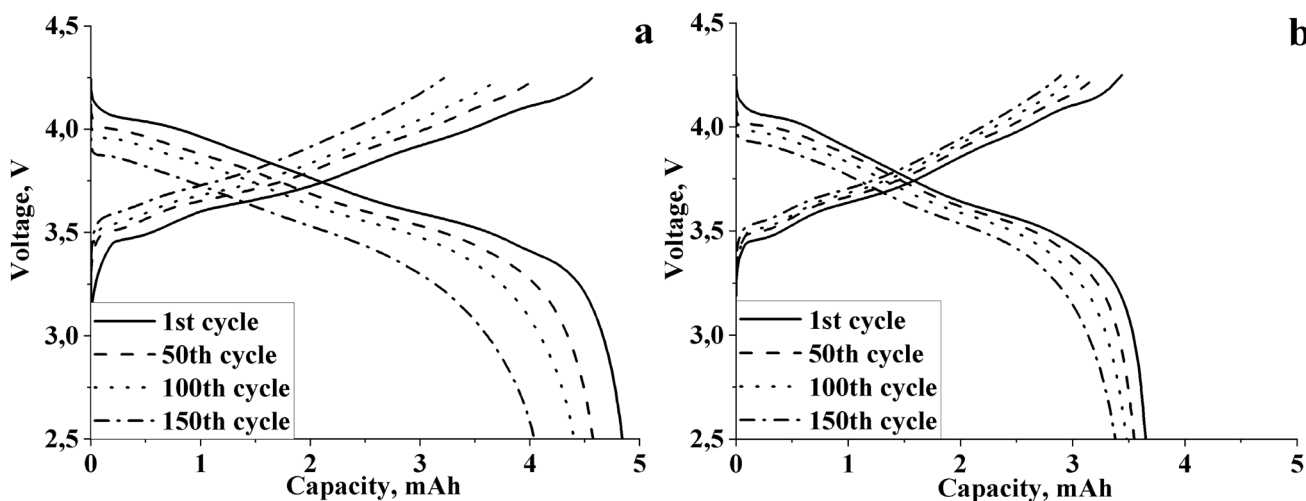**Fig. 12** Change of specific capacity of the pristine NMC and cathode materials with a protective layer of LATP during a long-term charge/discharge cycling at a current density of C/5: 1 pristine NMC; 2 NMC$_m$ (T); 3—NMC$_{sol-gel}$

Fig. 13 Charge/discharge curves for LIBs prototypes based on the pristine cathode material (**a**) and NMC$_{sol-gel}$ (**b**)
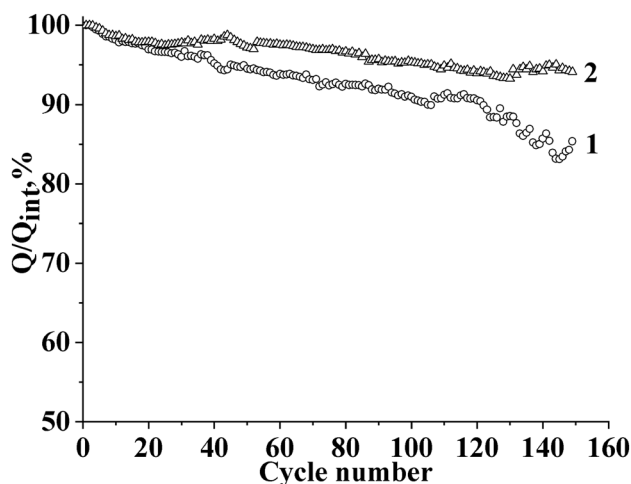
Fig. 14 Change of specific capacity of LIBs prototypes based on pristine NMC (1) and NMC$_{sol-gel}$ (2) during long-term charge/discharge cycling at current density C/5

stability of capacitive characteristics during long charge/discharge cycling, compared with LIBs prototypes based on the pristine cathode material.

4 Conclusions

The effect of the method of creating a protective layer on the surface of the NMC622 cathode material on its electrochemical characteristics was investigated for the first time in this work. It was found that the creation of a protective layer of nanoparticles of solid electrolyte LATP using two methods (mechanical application and sol–gel method) can increase the stability of the capacitive characteristics of the cathode material during a long-term charge–discharge cycling. However, applying the LATP protective layer to the particles of the NMC 622 cathode material by the sol–gel method is more promising technology, as it reduces the capacity drop during a long-term cycling by almost 2.5 times compared to the cathode material without a protective layer. In addition, the application of a protective layer of LATP using the sol–gel method can significantly increase the capacity of the cathode material at high current density. The obtained results provide a basis for a systematic study of the effect of the deposition of a protective LATP layer by the sol–gel method on the electrochemical characteristics of other layered cathode materials with the NMC-type structure.

Declarations

References

1. Wakayama H, Kawai Y (2017) The effect of the LiCoO$_2$/Li$_7$La$_3$Zr$_2$O$_{12}$ ratio on the structure and electrochemical properties of nanocomposite cathodes for all-solid-state lithium batteries. J Mater Chem A 5:18816–18822. https://doi.org/10.1039/C7TA05527G
2. Chebiam RV, Kannan AM, Prado F, Manthiram A (2001) Comparison of the chemical stability of the high energy density cathodes of lithium-ion batteries. Electrochem Commun 3:624–627. https://doi.org/10.1016/S1388-2481(01)00232-6
3. Yoshio M, Noguchi H, Itoh J et al (2000) Preparation and properties of LiCo$_y$Mn$_x$Ni$_{1-x-y}$O$_2$ as a cathode for lithium ion batteries. J Power Sour 90:176–181. https://doi.org/10.1016/S0378-7753(00)00407-9
4. Yoon CS, Park K-J, Kim U-H et al (2017) High-energy Ni-rich Li[Ni$_x$Co$_y$Mn$_{1-x-y}$]O$_2$ cathodes via compositional partitioning for next-generation electric vehicles. Chem Mater 29:10436–10445. https://doi.org/10.1021/acs.chemmater.7b04047
5. Wu L, Nam K-W, Wang X et al (2011) Structural origin of overcharge-induced thermal instability of Ni-containing layered-cathodes for high-energy-density lithium batteries. Chem Mater 23:3953–3960. https://doi.org/10.1021/cm201452q
6. Konishi H, Yoshikawa M, Hirano T (2013) The effect of thermal stability for high-Ni-content layer-structured cathode materials, LiNi$_{0.8}$Mn$_{0.1-x}$Co$_{0.1}$Mo$_x$O$_2$ (x= 0, 0.02, 0.04). J Power Sour 244:23–28. https://doi.org/10.1016/j.jpowsour.2013.05.004
7. Nguyen D-T, Kang J, Nam K-M et al (2016) Understanding interfacial chemistry and stability for performance improvement and fade of high-energy Li-ion battery of LiNi$_{0.5}$Co$_{0.2}$Mn$_{0.3}$O$_2$//silicon-graphite. J Power Sour 303:150–158. https://doi.org/10.1016/j.jpowsour.2015.10.089
8. Belharouak I, Lu W, Vissers D, Amine K (2006) Safety characteristics of Li(Ni$_{0.8}$Co$_{0.15}$Al$_{0.05}$)O$_2$ and Li(Ni$_{1/3}$Co$_{1/3}$Mn$_{1/3}$)O$_2$. Electrochem Commun 8:329–335. https://doi.org/10.1016/j.elecom.2005.12.007
9. Yoon W-S, Chung KY, McBreen J, Yang X-Q (2006) A comparative study on structural changes of LiCo$_{1/3}$Ni$_{1/3}$Mn$_{1/3}$O$_2$ and LiNi$_{0.8}$Co$_{0.15}$Al$_{0.05}$O$_2$ during first charge using in situ XRD. Electrochem Commun 8:1257–1262. https://doi.org/10.1016/j.elecom.2006.06.005
10. Cao H, Zhang Y, Zhang J, Xia B (2005) Synthesis and electrochemical characteristics of layered LiNi$_{0.6}$Co$_{0.2}$Mn$_{0.2}$O$_2$ cathode material for lithium ion batteries. Solid State Ionics 176:1207–1211. https://doi.org/10.1016/j.ssi.2005.02.023
11. Li J, Wang L, Zhang Q, He X (2009) Synthesis and characterization of LiNi$_{0.6}$Mn$_{0.4-x}$Co$_x$O$_2$ as cathode materials for Li-ion batteries. J Power Sour 189:28–33. https://doi.org/10.1016/j.jpowsour.2008.12.046
12. Kasnatscheew J, Evertz M, Kloepsch R et al (2017) Learning from Electrochemical data: simple evaluation and classification of

LiMO$_2$-type-based positive electrodes for Li-ion batteries. Energy Technol 5:1670–1679. https://doi.org/10.1002/ente.201700068

13. Kasnatscheew J, Evertz M, Streipert B et al (2017) Improving cycle life of layered lithium transition metal oxide (LiMO$_2$) based positive electrodes for Li ion batteries by smart selection of the electrochemical charge conditions. J Power Sour 359:458–467. https://doi.org/10.1016/j.jpowsour.2017.05.092

14. Myung S-T, Amine K, Sun Y-K (2010) Surface modification of cathode materials from nano-to microscale for rechargeable lithium-ion batteries. J Mater Chem 20:7074–7095. https://doi.org/10.1039/C0JM00508H

15. Wang K, Li X, Chen J (2015) Surface and interface engineering of electrode materials for lithium-ion batteries. Adv Mater 27:527–545. https://doi.org/10.1002/adma.201402962

16. Chen Y, Zhang Y, Chen B et al (2014) An approach to application for LiNi$_{0.6}$Co$_{0.2}$Mn$_{0.2}$O$_2$ cathode material at high cutoff voltage by TiO$_2$ coating. J Power Sour 256:20–27. https://doi.org/10.1016/j.jpowsour.2014.01.061

17. Hu S-K, Cheng G-H, Cheng M-Y et al (2009) Cycle life improvement of ZrO$_2$-coated spherical LiNi$_{1/3}$Co$_{1/3}$Mn$_{1/3}$O$_2$ cathode material for lithium ion batteries. J Power Sour 188:564–569. https://doi.org/10.1016/j.jpowsour.2008.11.113

18. Xiong X, Wang Z, Guo H et al (2013) Enhanced electrochemical properties of lithium-reactive V$_2$O$_5$ coated on the LiNi$_{0.8}$Co$_{0.1}$Mn$_{0.1}$O$_2$ cathode material for lithium ion batteries at 60 C. J Mater Chem A 1:1284–1288. https://doi.org/10.1039/C2TA00678B

19. Huang Y, Jin F-M, Chen F-J, Chen L (2014) Improved cycle stability and high-rate capability of Li$_3$VO$_4$-coated Li[Ni$_{0.5}$Co$_{0.2}$Mn$_{0.3}$]O$_2$ cathode material under different voltages. J Power Sour 256:1–7. https://doi.org/10.1016/j.jpowsour.2014.01.003

20. Yuan X, Xu Q, Liu X et al (2016) Layered cathode material with improved cycle performance and capacity by surface anchoring of TiO$_2$ nanoparticles for Li-ion batteries. Electrochim Acta 213:648–654. https://doi.org/10.1016/j.electacta.2016.07.157

21. Yang K, Fan L-Z, Guo J, Qu X (2012) Significant improvement of electrochemical properties of AlF$_3$-coated LiNi$_{0.5}$Co$_{0.2}$Mn$_{0.3}$O$_2$ cathode materials. Electrochim Acta 63:363–368. https://doi.org/10.1016/j.electacta.2011.12.121

22. Kobylianska S, Demchuk D, Khomenko V et al (2019) Surface Modification of the LiNi$_{0.5}$Co$_{0.2}$Mn$_{0.3}$O$_2$ Cathode by a Protective Interface Layer of Li$_{1.3}$Ti$_{1.7}$Al$_{0.3}$(PO$_4$)$_3$. J Electrochem Soc 166:A1920. https://doi.org/10.1149/2.0701908jes

23. Wu B, Wang S, Evans WJ IV et al (2016) Interfacial behaviours between lithium ion conductors and electrode materials in various battery systems. J Mater Chem A 4:15266–15280. https://doi.org/10.1039/C6TA05439K

24. Han X, Gong Y, Fu K et al (2017) Negating interfacial impedance in garnet-based solid-state Li metal batteries. Nat Mater 16:572–579. https://doi.org/10.1038/nmat4821

25. Zhao C-Z, Zhao B-C, Yan C et al (2020) Liquid phase therapy to solid electrolyte–electrode interface in solid-state Li metal batteries: a review. Energy Storage Mater 24:75–84. https://doi.org/10.1016/j.ensm.2019.07.026

26. Zhou D, Chen Y, Li B et al (2018) A stable quasi-solid-state sodium–sulfur battery. Angew Chemie Int Ed 57:10168–10172. https://doi.org/10.1002/anie.201805008

27. Xu B, Duan H, Liu H et al (2017) Stabilization of garnet/liquid electrolyte interface using superbase additives for hybrid Li batteries. ACS Appl Mater Interfaces 9:21077–21082. https://doi.org/10.1021/acsami.7b05599

28. Brünger AT (1992) Free R value: a novel statistical quantity for assessing the accuracy of crystal structures. Nature 355:472–475. https://doi.org/10.1038/355472a0

29. Qu X, Yu Z, Ruan D et al (2020) Enhanced electrochemical performance of Ni-rich cathode materials with Li$_{1.3}$Al$_{0.3}$Ti$_{1.7}$(PO$_4$)$_3$ coating. ACS Sustain Chem Eng 8:5819–5830. https://doi.org/10.1021/acssuschemeng.9b05539

30. Meng K, Wang Z, Guo H et al (2016) Improving the cycling performance of LiNi$_{0.8}$Co$_{0.1}$Mn$_{0.1}$O$_2$ by surface coating with Li$_2$TiO$_3$. Electrochim Acta 211:822–831. https://doi.org/10.1016/j.electacta.2016.06.110

31. Xu Y-D, Xiang W, Wu Z-G et al (2018) Improving cycling performance and rate capability of Ni-rich LiNi$_{0.8}$Co$_{0.1}$Mn$_{0.1}$O$_2$ cathode materials by Li$_4$Ti$_5$O$_{12}$ coating. Electrochim Acta 268:358–365. https://doi.org/10.1016/j.electacta.2018.02.049

32. Tang W, Chen Z, Xiong F et al (2019) An effective etching-induced coating strategy to shield LiNi$_{0.8}$Co$_{0.1}$Mn$_{0.1}$O$_2$ electrode materials by LiAlO$_2$. J Power Sour 412:246–254. https://doi.org/10.1016/j.jpowsour.2018.11.062

33. Ma S, Jiang M, Tao P et al (2018) Temperature effect and thermal impact in lithium-ion batteries: a review. Prog Nat Sci Mater Int 28:653–666. https://doi.org/10.1016/j.pnsc.2018.11.002

34. David L, Mohanty D, Geng L et al (2019) High-voltage performance of Ni-Rich NCA cathodes: linking operating voltage with cathode degradation. ChemElectroChem 6:5571–5580. https://doi.org/10.1002/celc.201901338

35. Kang IS, Lee Y-S, Kim D-W (2013) Improved cycling stability of lithium electrodes in rechargeable lithium batteries. J Electrochem Soc 161:A53. https://doi.org/10.1149/2.029401jes